arXiv:2405.19882v3 [cs.CV] 24 Oct 2024

PixOOD: Pixel-Level Out-of-Distribution Detection

Tomáš Vojíř, Jan Šochman, and Jiří Matas

Czech Technical University in Prague, Faculty of Electrical Engineering
Department of Cybernetics, Visual Recognition Group
{tomas.vojir, jan.sochman, matas}@fel.cvut.cz

Abstract. We propose a pixel-level out-of-distribution detection algorithm, called PixOOD, which does not require training on samples of anomalous data and is not designed for a specific application which avoids traditional training biases. In order to model the complex intra-class variability of the in-distribution data at the pixel level, we propose an online data condensation algorithm which is more robust than standard K-means and is easily trainable through SGD. We evaluate PixOOD on a wide range of problems. It achieved state-of-the-art results on four out of seven datasets, while being competitive on the rest. The source code is available at `https://github.com/vojirt/PixOOD`.

Keywords: Out-of-distribution · Anomaly · Data condensation · Expectation maximization

1 Introduction

State-of-the-art methods for many computer vision tasks rely on machine learning and therefore on the properties of the training data; consider segmentation, recognition, detection, optical flow, tracking, monocular depth estimation *etc.*. In the laboratory setting, when the training and test sets are obtained by a random split of the available corpus, the standard machine learning assumption of identical data distribution is satisfied by construction. However, in real-world deployment of computer vision systems, encountering domain shifts and out-of-distribution (OOD) data is unavoidable, as when a new product appears (recognition), new material is introduced (segmentation) or a unique 3D structure built (monocular depth estimation).



Fig. 1: Examples of PixOOD results for road, maritime and industrial anomaly detection tasks. PixOOD is able to identify anomalous data not even considered, *i.e.* not labelled, in standard benchmarks, *e.g.* power cables (not in Cityscapes training classes) or spilled-out content or scratches in insulation.

To be robust, computer vision methods need to address the problem of recognising OOD inputs, *i.e.* data not represented in the training set. Otherwise, for

such data, their output is at best not guaranteed, at worst arbitrary, potentially disastrous. Besides the potential for reliable performance, methods that perform OOD, may benefit from human-in-the-loop intervention on novel data, often integrating collection of OOD or rare data for annotation.

In this paper, we present PixOOD, a novel method for out-of-distribution data detection at the level of pixels. The approach is general, it does not require training on samples of anomalous data, nor on synthetically generated outlier data, which requires rather specific knowledge of OOD data properties. These might be known in some case, but we aim at the scenario where minimal assumptions are made about the data not presented during training – such data cannot be synthesized. The proposed method does not exploit constraints that hold in specific applications like industrial inspection or road anomaly, or a particular problem setting like open set semantic segmentation. Fig. 1 shows examples from three diverse ODD benchmarks PixOOD is evaluated on in Sec. 4: the MVTec AD [2], a batch of industrial anomaly detection problems; the SMIYC [7] which contains three sub-tracks: a road anomaly detection (general anomaly segmentation in full street scenes), obstacle detection (obstacle segmentation with the road as region of interest), and LostAndFound; and finally the LaRS benchmark [45], a maritime obstacle segmentation problem with examples of obstacles provided.

The inspiration for our method is the recently published GROOD [40] approach for image-level classification and OOD detection. We particularly appreciate its simplicity and calibrated OOD score that is a result of solving the Neyman-Pearson task [28, 29] in a low dimensional projection space. However, several shortcomings of the GROOD method limit its applicability to diverse OOD problems. Specifically, two major issues are (i) pixel-level generalisation (*i.e.* decision making for each pixel instead of the whole image) which poses several engineering challenges and (ii) limited capability of complex intra-class variability modelling, which naturally arises in the pixel-level domain.

We address these weaknesses in PixOOD and demonstrate its efficacy on various downstream tasks. We show that in the case of pixel-level OOD decision problems with large intra-class variations the GROOD single mean representation is not sufficient. We propose a novel data condensation algorithm for rich class appearance modelling. The condensation method is derived from the K-means algorithm. We show it is related to a complete data log likelihood optimisation through the EM algorithm. The proposed method is more robust than the standard K-means and it is easily trained on large volumes of data through stochastic gradient descent. The condensation method is general and of interest on its own. We also introduce several architectural improvements to accommodate the requirements of the pixel-level decision tasks. The contributions of the paper are summarised as follows:

1. A novel pixel-level OOD detection method called PixOOD. The approach is general (*i.e.* not designed for specific task/benchmark) and does not require any OOD training samples neither real nor synthetic (Sec. 3).
2. A novel data condensation algorithm formulated as a stochastic optimisation with a novel loss function and re-initialisation mechanism (Sec. 3.1).

3. We theoretically show the relation of the condensation loss function to a lower bound of the complete data log-likelihood optimisation (Sec. 3.1).
4. We demonstrate the applicability of the proposed method through applying it on three diverse benchmarks which are typically solved independently by specialised methods. The proposed method performs competitively on all (seven) datasets achieving state-of-the-art results on four (Sec. 4).

2 Related Work

On the very basic level we divide the methods to those which use real-world or synthetic OOD data [6,8,11,14–16,25,27,34,37,43] and those which do not [3,13, 17,22–24,27,37–39]. In our view, using a proxy for OOD data (*e.g.* objects from COCO in road anomaly [27,34] or synthetic textures in industrial inspection [43]) is the same as making an assumption about the form of allowed anomalies, which goes against the definition of the word 'anomaly' itself. We aim at a method applicable to the widest possible spectrum of problems, thus avoid introducing task specific biases through auxiliary (synthetic) OOD data.

Among the methods we compare with, one can observe several trends. In the road anomaly detection community, the reconstructions methods [23, 24, 38, 39] are trained, to reconstruct "normal" pixels. The assumption is that during inference an anomalous object would be poorly reconstructed which could be detected. These pixel-level reconstruction-based method were slowly overtaken by energy-based models [8, 15, 17] that introduce regularisation to the classification objective loss to enforce particular predictions for anomalous pixels, *e.g.* uniform distribution of posterior probability over in-distribution (ID) classes. Recently, region-based methods [16, 27, 34, 44] gained popularity. This makes the ID/OOD reasoning more robust to noise and makes sense in this domain since most anomalous objects in driving scenarios have strong boundary separation from its surrounding. The region-based methods, however, are not common in other domains such as the industrial anomaly detection where the anomalies have different characteristics, *e.g.* deformations or missing parts.

In industrial anomaly benchmarks, recent successful methods are still based on reconstruction [26, 42, 43], likelihood modelling [1, 19] or nearest-neighbour classification [35]. Interestingly, only the latest methods start to depart from a single model for each class and start to focus on a general models [26, 42]. A possible reason is that the benchmarks are rather small and images are taken under well controlled conditions, so the generalisation is not the prime objective.

3 Method

In this section we describe the proposed PixOOD method for OOD (anomaly) detection at the pixel level. The PixOOD framework consists of three components (illustrated in Fig. 2): (i) extraction of the pixel/patch feature representation, (ii) building a two-dimensional projection space, and (iii) finding the optimal and calibrated ID/OOD decision strategy. The framework is similar to [40],

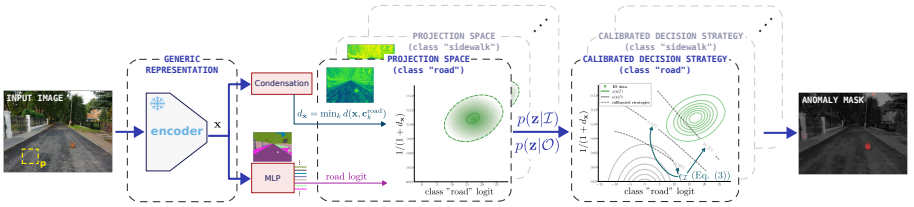


Fig. 2: PixOOD inference overview. Individual steps are described in Sec. 3. Note that the condensation is run independently for each class during training while MLP is trained jointly for all classes.

which however is not applicable to pixel-level tasks due to issues discussed and addressed in Sec. 3.3, and it is experimentally validated in Sec. 4.1.

Representation. Every patch $\mathbf{p}$ in the input image (the patch size, in our case, is determined by the ViT [12] architecture) is first transformed into a feature vector $\mathbf{x} \in \mathbb{R}^D$ by a fixed pre-trained model. This representation needs to be rich enough to allow modelling ID data in a given pixel-level vision tasks. A good example of such model is the self-supervised trained DINOv2 encoder [30] that we employ in this work. Similarly, methods such as [18,40,41] utilized pre-trained CLIP [33] image encoder for image-level OOD detection tasks.

2D Projection Space. The 2D projection space serves two purposes: First, it makes it possible to estimate the ID densities with potentially limited data (*e.g.* ∼200 samples per class for MVTecAD dataset), second, it allows to make reasonable assumptions about the unknown OOD distribution, which would be difficult/impossible in the encoder's high-dimensional space.

As opposed to the image-level task [40], the pixel/patch-level representations tend to produce more complex distributions in the (1024-dim in our case) embedding space over an image-level semantic classes. We observed that the simple projections used in [40] is not able to model the rich intra-class appearance variations, *e.g.* imagine pixels (patches) corresponding to car label may be visually drastically different (wheels vs. windshield) as shown in the ablation study in Sec. 4. Thus we replace the first projection, the Linear Probe, with a multi-layer Perceptron (Sec. 3.2) and instead of the nearest class mean projection we propose to use our novel data condensation algorithm (Sec. 3.1). The condensation method is general and may find its uses also outside of the PixOOD method. The projection space is thus formed (for each class independently) as $\mathcal{Z} = \mathcal{Z}_{\text{MLP}} \times \mathcal{Z}_{\text{N}c_k}$, where $\mathcal{Z}_{\text{MLP}}$ is a 1-D space of MLP logit scores for the particular class and $\mathcal{Z}_{\text{N}\mathbf{c}_k}$ is a 1-D space of distances to the nearest class etalon found by the condensation algorithm.

Decision Strategy. The optimal decision strategy is found independently in all these 2D projection spaces. Let $\mathcal{I}$ be a (meta-)class representing the in-distribution samples from a target class and $\mathcal{O}$ a (meta-)class for out-of-distribution data. Both, $p(\mathbf{z}|\mathcal{I})$ and $p(\mathbf{z}|\mathcal{O})$ are modelled as multivariate normal distributions in $\mathbf{z} \in \mathcal{Z}$. The parameters of $p(\mathbf{z}|\mathcal{I})$ are estimated from the training data and

$p(\mathbf{z}|\mathcal{O})$ is constructed with zero mean and a diagonal covariance matrix with large variances (see [40] for detailed reasoning about the OOD distribution).

The ID/OOD classification problem is formulated, same as in [40], as a Neyman-Pearson task [28, 36]: Find a strategy $q^*(z) : \mathcal{Z} \to \{\mathcal{I}, \mathcal{O}\}$ such that

$$\begin{aligned} q^* = \arg\min_q \int_{\mathbf{z}:q(\mathbf{z})\neq\mathcal{O}} p(\mathbf{z}|\mathcal{O})\, d\mathbf{z} \\ \text{s.t.} \quad \epsilon_{\mathcal{I}} = \int_{\mathbf{z}:q(\mathbf{z})\neq\mathcal{I}} p(\mathbf{z}|\mathcal{I})\, d\mathbf{z} \leq \epsilon \end{aligned} \tag{1}$$

This optimisations problem minimises the false positive rate (false acceptance of OOD data) and bounds the ID false negative rate by ϵ. It is known [36] that the optimal strategy for a given $\mathbf{z} \in \mathcal{Z}$ is constructed using the likelihood ratio:

$$q(\mathbf{z}) = \begin{cases} \mathcal{I} & \text{if} \quad r(\mathbf{z}) > \mu \\ \mathcal{O} & \text{if} \quad r(\mathbf{z}) \leq \mu \end{cases} \quad \text{where} \quad r(\mathbf{z}) = \frac{p(\mathbf{z}|\mathcal{I})}{p(\mathbf{z}|\mathcal{O})} \tag{2}$$

The optimal strategy q^* is obtained by selecting maximal threshold μ s.t. $\epsilon_{\mathcal{I}} \leq \epsilon$.

ID/OOD Score. In practice, we would specify the acceptable false negative rate ϵ and obtain a single optimal strategy. However, most evaluation benchmarks require a score in the range $(0, 1)$ which is then used to compute the evaluation metrics by varying a threshold on this score. To produce such score, we follow [40] and learn a mapping from the likelihood ratio to false negative rate. We uniformly cover the projection space $\mathcal{Z}$ by M samples, and for each sample we find the likelihood ratio $r(\mathbf{z}_i)$ and a corresponding error $\epsilon^i_{\mathcal{I}}$ for the threshold set to $\mu = r(\mathbf{z}_i)$. This results in a set of pairs $R = \{(r(\mathbf{z}_i), \epsilon^i_{\mathcal{I}})\}_{i=1}^M$. We build an in-distribution scoring function $s_{\mathcal{I}}$ as a linear interpolation function over $\mathcal{Z}$ estimated from R such that

$$s_{\mathcal{I}}\left(r(\mathbf{z}_i)\right) \approx \epsilon^i_{\mathcal{I}} \tag{3}$$

This score corresponds to the false negative error that we would make on the in-distribution data if we selected $\mu = r(\mathbf{z})$ in the optimal strategy q^* (Eq. (2)).

Finally, we define the OOD ("anomaly") score as

$$s_{\mathcal{O}}\left(r(\mathbf{z})\right) = 1 - s_{\mathcal{I}}\left(r(\mathbf{z})\right) \tag{4}$$

The score $s_{\mathcal{O}}$ is used in all experiments as the output of the PixOOD method. It is in the desired $(0, 1)$ range, it is calibrated and explainable and with a clear meaning corresponding to the false negative rate on the ID data. See the decision boundaries in Fig. 2 for illustration of the effect of $\epsilon_{\mathcal{I}}$. Note that the usable range of this score is at the tail of the range, *e.g.* ≥ 0.95 which is equivalent to saying that the false negative error of the ID data is $\leq 5\%$. See $\epsilon_{\mathcal{I}}$, Eq. (3), and its corresponding decisions boundaries in Fig. 2 for illustration.

3.1 Incremental Soft-to-Hard Data Condensation

Instead of using a single etalon for each class as in [40], the PixOOD method uses up to K etalons per class. Due to the amount of data (pixels), the etalons have

to be estimated incrementally (using batches of data), ideally in a stochastic gradient descent framework. We first motivate and formulate the optimisation criterion for condensing a (single class) dataset into a set of K etalons. We then show that the soft-assignment condensation criterion corresponds closely to the EM-algorithm steps when finding the optimal parameters of a spherical Laplace distribution mixture model. This gives us more formal view of the condensation criterion. Finally, we show how to alleviate the issue of the local minima.

Let $T = \{\mathbf{x}_i \in \mathcal{X} \equiv \mathbb{R}^D\}_{i=1}^N$ be a (potentially large) dataset of training samples from one class. The dimensionality of the samples depends on the representation used (later we use $D = 2$ and $D = 1024$). The **dataset condensation task** is to find up to K etalons (representatives) $\mathbf{c}_1, \ldots, \mathbf{c}_K$ ($\mathbf{c}_k \in \mathcal{X}$) that cover the training data, *i.e.* all data points should be close to an etalon. The number of etalons is not fixed, but is upper-bounded by K (a "budget"). Further, each etalon should represent a similar portion of the data.

Let us denote the trainable parameters, *i.e.* the etalon coordinates, $\mathbf{c} = (\mathbf{c}_1, \ldots, \mathbf{c}_K)$ and let $d(\mathbf{x}, \mathbf{c}_k)$ be the L_2 distance between a data point $\mathbf{x}$ and an etalon $\mathbf{c}_k$. K-means optimises

$$\mathbf{c}^* = \arg\min_{\mathbf{c}} \frac{1}{N} \sum_{i=1}^{N} \min_k d(\mathbf{x}_i, \mathbf{c}_k)^2 \ . \tag{5}$$

This objective is not smooth due to the hard assignment to the closest etalon. Also, K-means tends to get stuck in local minima and is known to be sensitive to outliers in data due to the square of the distance. To make the criterion smooth, we use a smooth approximation [9] of the min operator:

$$\mathbf{c}^* = \arg\min_{\mathbf{c}} \frac{1}{N} \sum_{i=1}^{N} \sum_{k=1}^{K} w(k, i; \tau) d(\mathbf{x}_i, \mathbf{c}_k)^2 \tag{6}$$

$$w(k, i; \tau) = \frac{\exp\left(-d(\mathbf{x}_i, \mathbf{c}_k)^2 / \tau\right)}{\sum_{j=1}^{K} \exp\left(-d(\mathbf{x}_i, \mathbf{c}_j)^2 / \tau\right)} \ , \tag{7}$$

where Eq. (7) is the softmin function with temperature scaling τ. The temperature scaling allows a smooth transition from a soft assignment (easier to optimise, less susceptible to local minima) and a hard assignment (the goal of condensation). During the optimisation, the value of τ is scheduled to decrease from a large (soft assignment) to a low value (hard assignment).

The smooth objective in Eq. (6) is sensitive to outliers in data due to the square of the distance. When removing the square from Eq. (5), the solution to the problem is known as the K-medians algorithm which requires an iterative optimisation for finding the medians in each step. Instead, we remove the square in the smoothed version Eqs. (6) and (7) which is still easy to optimise and

allows the soft-hard assignment transition through τ parameter:

$$\mathbf{c}^* = \arg\min_{\mathbf{c}} \frac{1}{N} \sum_{i=1}^{N} \sum_{k=1}^{K} w(k,i;\tau) d(\mathbf{x}_i, \mathbf{c}_k) \tag{8}$$

$$w(k,i;\tau) = \frac{\exp\left(-d(\mathbf{x}_i, \mathbf{c}_k)/\tau\right)}{\sum_{j=1}^{K} \exp\left(-d(\mathbf{x}_i, \mathbf{c}_j)/\tau\right)} \tag{9}$$

The final requirement of the condensation task is that each etalon covers approximately the same number of data points. To that end, each etalon is assigned a trainable scale parameter $\boldsymbol{\beta} = (\beta_1, \ldots, \beta_K)$ to make it adaptive to the varying local data density. Instead of just dividing the distance by the parameter $(d(\mathbf{x}_i, \mathbf{c}_k)/\beta_k)$ in the formula, which would have a trivial minimiser for $\beta_k = \infty$, the distance is replaced by a logarithm of the Laplace distribution which regularises the β_k parameter to avoid this degenerated solution. This gives us the final loss optimised by the proposed algorithm:

$$L(\mathbf{c}, \boldsymbol{\beta}; T, \tau) = -\frac{1}{N} \sum_{i=1}^{N} \sum_{k=1}^{K} w(k,i;\tau) \log\left(\frac{1}{\beta_k} e^{-\frac{d(\mathbf{x}_i, \mathbf{c}_k)}{\beta_k}}\right), \tag{10}$$

where $w(k,i;\tau)$ is defined in Eq. (9). The full iterative soft-hard condensation algorithm is summarised in Fig. 3 (right) and the individual steps in its derivation are illustrated on toy example in Fig. 3 (left).

Relation to EM Algorithm. Interestingly, this objective has another interpretation. It is a lower bound on the complete data log-likelihood in EM algorithm for a mixture of spherical Laplace distributions with equal priors. Let us model the measurements $\mathbf{x}$ by a spherical Laplace distribution mixture model

$$p(\mathbf{x}; \boldsymbol{\pi}, \boldsymbol{c}, \boldsymbol{\beta}) = \sum_{k=1}^{K} \pi_k p(\mathbf{x}|k; \mathbf{c}_k, \beta_k) = \sum_{k=1}^{K} \pi_k \frac{1}{Z_k} \frac{1}{\beta_k^{D-1}} \exp\left(-\frac{d(\mathbf{x}, \mathbf{c}_k)}{\beta_k}\right) \tag{11}$$

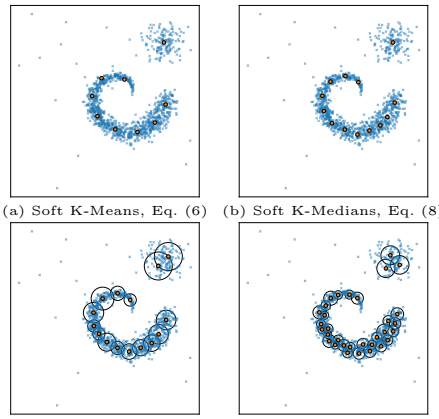
where $\boldsymbol{\pi} = (\pi_1, \ldots, \pi_K)$ are the prior probabilities of each component, $\mathbf{c} = (\mathbf{c}_1, \ldots, \mathbf{c}_K)$ and $\boldsymbol{\beta} = (\beta_1, \ldots, \beta_K)$ characterise the component distributions as in Eq. (10) and Z_k's are the normalising factors of the spherical Laplace distribution independent of $\boldsymbol{\beta}$ and $\mathbf{c}$. The EM maximises the complete data log-likelihood

$$\mathcal{L}(\boldsymbol{\pi}, \boldsymbol{c}, \boldsymbol{\beta}; T) = \sum_{i=1}^{N} \log p(\mathbf{x}; \boldsymbol{\pi}, \boldsymbol{c}, \boldsymbol{\beta}) = \sum_{i=1}^{N} \log \sum_{k=1}^{K} \pi_k p(\mathbf{x}|k; \mathbf{c}_k, \beta_k) \,. \tag{12}$$

By introducing a variational distribution $w(k,i)$ (we show how to choose it below) a lower bound to $\mathcal{L}$ is derived using Jensen's inequality as

$$\mathcal{L}(\boldsymbol{\pi}, \boldsymbol{c}, \boldsymbol{\beta}; \mathbf{x}) = \sum_{i=1}^{N} \log \sum_{k=1}^{K} w(k,i) \frac{\pi_k p(\mathbf{x}|k; \mathbf{c}_k, \beta_k)}{w(k,i)} \tag{13}$$

$$\geq \sum_{i=1}^{N} \sum_{k=1}^{K} w(k,i) \log \frac{\pi_k p(\mathbf{x}|k; \mathbf{c}_k, \beta_k)}{w(k,i)} \tag{14}$$



(a) Soft K-Means, Eq. (6) (b) Soft K-Medians, Eq. (8)

(c) Condensation, Eq. (10) (d) Eq. (10) + re-inits

Given: $T = \{x_i \in \mathbb{R}^D\}_{i=1}^N$
Initialise: $\mathbf{c}, \boldsymbol{\beta}, \tau, q, \lambda$
for epoch < num. epochs **do**
  for $X = \{\mathbf{x}_i\}_{i=1}^n \subset T$ **do** ▷ iterate over batches
    Compute $d(\mathbf{x}_i, \mathbf{c}_k)$ $\forall \mathbf{x}_i \in X, \forall \mathbf{c}_k \in \mathbf{c}$
    Compute $w(k, i; \tau)$ ▷ Eq. (9)
    Compute $L(\mathbf{c}, \boldsymbol{\beta}; T, \tau)$ ▷ Eq. (10)
    $\forall \mathbf{c}_k : \mathbf{c}_k \leftarrow \mathbf{c}_k - \lambda \frac{\partial L}{\partial \mathbf{c}_k}$
    $\forall \beta_k : \beta_k \leftarrow \beta_k - \lambda \frac{\partial L}{\partial \beta_k}$
    Update $s_t(k)$ ▷ Eq. (18)
  end for
  if epoch > $\text{epoch}_{\text{warmup}}$ and $s_t(k) < \theta_r$ **then**
    Re-initialise $\mathbf{c}_k$
  end if
  $\tau \leftarrow$ cos_scheduler(epoch)
end for

Fig. 3: Left: Methods derived in Sec. 3.1 applied to synthetic data (blue crosses) with outliers (isolated blue crosses). Only the "useful" etalons (from total of 50) with $s_t(k) >= \theta_r$ are displayed as orange circles. (a) K-means is sensitive to outliers and most etalons converge towards isolated data points (not shown) – only 9 useful etalons. (b) K-medians is more robust – 13 useful, (c) condensation adds the scale parameter β_k to each cluster (black circle) enabling adaptive region of influence – 15 useful, (d) re-inits with *(c)* preserve significantly more etalons by combining re-initialization strategy with adaptive scale – 32 useful. **Right:** Iterative soft-hard condensation algorithm summary.

which for the case of a mixture of spherical Laplace distributions looks like

$$\sum_{i=1}^{N}\sum_{k=1}^{K} w(k,i)\log\pi_k + w(k,i)\log\frac{1}{\beta_k^{D-1}}\exp\left(-\frac{d(\mathbf{x}_i,\mathbf{c}_k)}{\beta_k}\right) - w(k,i)\log w(k,i)\ . \tag{15}$$

Since the M-step maximises this lower bound only over $\mathbf{c}$ and $\boldsymbol{\beta}$, the last term becomes a constant and could be omitted from the optimisation. Further, if all priors π_k are assumed constant $\pi_k = 1/K$, also the first term disappears. What is left is maximisation of the negative of the loss (10). In the E-step any variational distribution $w(k,i)$ defines a lower bound for $\mathcal{L}$. It is easy to show that the optimal $w^*(k,i) = p(k|\mathbf{x}; \boldsymbol{\pi}, \boldsymbol{c}, \boldsymbol{\beta})$. Using the Bayes formula

$$w^*(k,i) = \frac{p(\mathbf{x}_i; \boldsymbol{\pi}, \boldsymbol{c}, \boldsymbol{\beta})}{\sum_{j=1}^K p(\mathbf{x}_i; \boldsymbol{\pi}, \boldsymbol{c}, \boldsymbol{\beta})} = \frac{\frac{1}{\beta_k^{D-1}}\exp\left(-\frac{d(\mathbf{x}_i,\mathbf{c}_k)}{\beta_k}\right)}{\sum_{j=1}^K \frac{1}{\beta_j^{D-1}}\exp\left(-\frac{d(\mathbf{x}_i,\mathbf{c}_j)}{\beta_j}\right)}\ , \tag{16}$$

where the constant a priori probabilities cancel out. Although optimal, when the embedding dimension D is high (*e.g.* 1024), this formula becomes numerically unstable. Replacing all β_k's by a constant value τ reduces the formula into Eq. (9). This in principle breaks the EM monotonicity convergence property, but practically avoids the numerical instability and allows for independent

treatment of the etalon scale parameters and the soft-to-hard transition parameter τ. In practice, EM converges to local maxima only even with the optimal lower bound, so we solve both problems by introducing etalon re-inits.

Re-Inits. K-means, EM algorithm and also the proposed condensation algorithm converges, in general, to a local optimum. The soft-hard scheduling helps to alleviate this to some extent, but the result still depends on the initialisation. Although there exist heuristic initialisation methods like K-means++, they are computationally expensive. Hence, we introduce etalon re-inits inside the optimisation loop. For each etalon, we compute its data sample (batch) support as

$$s(k) = \sum_{i=1}^{N} w(k, i; \tau) \ . \tag{17}$$

In the EM interpretation, this corresponds to a posteriori probability of the mixture component given data (multiplied by N). A small support is indicative of a misplaced etalon. In the stochastic optimisation, the mini-batch data samples are often small and biased resulting in noisy $s(k)$ estimate. Thus, we estimate the support using init-unbiased running exponential weighted average [21] over mini-batches. Given a decay rate q, at the iteration t it is estimated as

$$s_t(k) = (1 - q_t)s_{t-1}(k) + q_t s(k) \quad \text{where} \quad q_t = q \,/\, \big(1 - (1 - q)^t\big) \,. \tag{18}$$

An etalon is reset if, after a warm-up number of iterations, its $s_t(k) < \theta_r$. The θ_r is user-defined threshold and it controls the balance between number of used etalons and coverage of low density areas (we set it to 1 in all experiments). We reset the etalon to a random data point from the mini-batch and add a little noise to avoid degenerate configurations.

3.2 Discriminative Classifier

The discriminative power of simple Linear Probing (LP) technique, used in [40], is inadequate for the more complex pixel-level classification task. The LP is generally used to assess zero-shot performance of large pre-trained model on image classification task and most often is implemented as a linear regression using off-the-shelf solver (*e.g.* L-BFGS [32]) that requires all data at the same time. However, this techniques are prohibitive in pixel domain due to sheer amount of data. Thus, we propose to replace the LP by a small multi-layer Perceptron (MLP) network consisting of two layers with GELU [20] non-linearity. That increases the representation power and is easy to use in the batch processing regime with increased volume of data of the pixel domain.

3.3 Pixel-Level Adaptations

The pixel-level tasks bring two extra technical challenges: mixed patches and need for up-scaling. Both are consequence of using ViT [12] architecture as a

backbone and its first processing step, splitting the input into patches. Inevitably, some patches contain more than one pixel-level semantic label (*e.g.* patch on boundary of road and sidewalk will contain labels of both classes). Although they are relatively rare, we observed their negative impact on the training of the condensation algorithm. Thus we consider only patches with more than 90% of one class label during training. At test time, all patches are processed equally. Note that the training of the MLP is performed on the original input resolution by up-scaling the MLP output logits, which is a common approach, and thus the mixed patches have no effect.

PixOOD as described, works with patches and thus on a lower than original resolution. To obtain the final full resolution OOD score we follow the common practice and upscale the output score map. Further, we found out that up-scaling the encoder's feature maps at the inference time (but *not* during training) works better than only up-scaling the final OOD scores as ablated in Sec. 4.1.

4 Experiments

In all experiments, the proposed PixOOD uses no anomaly or OOD data during training (such as auxiliary datasets or synthetic anomalies through augmentation) except for the LaRS dataset where the obstacle class is part of training data. We use frozen DINOv2 [30] ViT-L variant as a backbone in all experiments and train using AdamW optimizer: the condensation algorithm (100 epochs, starting learning rate 0.1 with cosine decay and 'budget' K set to 1000), classification MLP (30 epochs with learning rate 0.0001). The final calibrated strategy is found on available training data for respective task. Qualitative results with typical failure cases are shown in Figs. 1 and 4 and more examples are provided in supplementary material. All training was done on a single NVIDIA A100-40GB. The runtime of the condensation algorithm for CityScapes dataset and for all classes was 5, 8 and 17 hours for K equal to 200, 500 and 1000 respectively.

Datasets. Commonly used benchmarks from recent literature for the respective domains are used: (i) for the road anomaly detection, where the evaluation is limited to the road region only – Road Anomaly [24], FischyScapes LaF [4, 31], SMIYC [7] (Obstacle Track, LaF NoKnown), (ii) for semantic segmentation anomaly – SMIYC (Anomaly Track), (iii) for industrial inspection – MVTec AD [2] and (iv) for maritime obstacle detection – LaRS [45].

Evaluation metrics. We use metrics standard for the respective tasks. For road and semantic segmentation anomaly detection, the commonly used metrics are Average Precision (AP) – area under precision-recall curve, False Positive Rate at 95% of True Positive Rate, denoted simply as FPR, and mean F1 score computed component-wise and averaged over different detection thresholds. In the industrial inspection domain, image and pixel level AUROC – area under ROCs curve are most often used together with AUPRO used in [2] – per-region overlap (PRO), to account for anomalies of different sizes within one image. The maritime obstacle detection (LaRS) uses standard mean Intersection over Union (mIoU) for the semantic classes and a domain specific metrics [5] such as: 1) wa-

Table 1: Ablation study – novel condensation, "budget" K, and pixel adaptation techniques. All reported results use the best performing setup of the PixOOD pipeline except one change that is being ablated. Components of the best setup are highlighted in green.

PixOOD with	K	RA+FS+RO	
		mean AP ↑	mean FPR ↓
Single Mean	1	88.14	3.49
Soft K-Means – Eq. (6)	200	93.01	2.26
Soft K-Medians – Eq. (8)	200	93.54	1.99
Soft-to-Hard Cond. – Sec. 3.1	200	94.11	1.82
	500	94.71	1.67
	1000	94.80	1.64
Linear Probe		92.36	2.38
Multi-Layer Perceptron		94.80	1.64
Patch label percentage > 50%		94.22	1.77
Patch label percentage > 90%		94.80	1.64
Feature map up-sampling × 1		92.14	2.35
Feature map up-sampling × 2		94.20	1.75
Feature map up-sampling × 5		94.78	1.65
Feature map up-sampling × 7		94.80	1.64

Table 2: Comparison with state-of-the-art methods on Road Anomaly and FS LaF datasets. The gray-out lines show additional results of the DaCUP method with DINOv2 backbone and a *meta*-method obtained by combining PixOOD with road-anomaly specialised method DaCUP [39] (for details see Sec. 4.2).

Method	OOD Data	Road Anomaly		FishyScapes LaF	
		AP ↑	FPR ↓	AP ↑	FPR ↓
SynBoost [11]	✓	63.72	52.27	92.46	❷ 0.66
PEBAL [37]	✓	67.31	39.41	84.05	1.58
Maximized Entropy	✓	❷ 96.23	❷ 6.03	77.16	10.14
RbA [27]	✓	92.99	9.01	85.98	2.87
Mask2Anomaly [34]	✓	94.10	16.91	❶ 94.49	❶ 0.52
EAM [16]	✓	❶ 96.43	❶ 2.26	❷ 93.67	0.77
Image Resynthesis [24]	✗	76.39	48.08	66.75	3.10
EAM [16]	✗	88.96	17.89	64.86	16.73
RbA [27]	✗	89.76	16.54	74.70	15.13
JSR-Net [38]	✗	94.42	9.25	78.30	3.96
DaCUP [39]	✗	❷ 96.19	❷ 5.46	❷ 89.75	❷ 1.45
PixOOD (**Ours**)	✗	❶ 96.39	❶ 4.30	❶ 93.55	❶ 0.54
DaCUP++ (CityScapes)	✗	98.24	3.04	93.23	0.57
Ours+DaCUP (recon.)	✗	98.66	2.12	94.66	0.30

teredge accuracy – computed from boundary between water and static obstacles and (2) obstacle detection accuracy – precision, recall and F1 score where the true positive detections are considered if predicted obstacle covers the ground-truth pixels from more than 70%. The final ranking in LaRS is determined by the Q measure which is computed as F1 × mIoU.

4.1 Ablation Study

We use road anomaly detection as the downstream task on which we demonstrate the effectiveness of the proposed condensation algorithm and the effect of different 'budget' size K. All hyper-parameters and random seeds for different variants of the method were fixed.

The results for both these ablations are presented in Tab. 1. They show that a single mean representation is insufficient for complex class modelling in pixel-level domain. Furthermore, robustness and efficacy of the proposed condensation method is demonstrated by increased performance compared to K-{Means, Medians} algorithms. The performance can be further improved by allowing larger 'budget' K and it saturates for K around 1000 suggesting that the proposed method can utilise extra clusters, up to a saturation point, efficiently.

Furthermore, we evaluate the proposed generalisations and technical improvements from Sec. 3.3. Note that for *Linear Probe* we used single fully connected layer and trained it by SGD, since it can be processed in batches as discussed in Sec. 3.2. Results are presented in a leave-one-out manner in the bottom three blocks of Tab. 1. By modifying only one part and leaving the rest in the best configuration it clearly shows the benefit of every design choice.

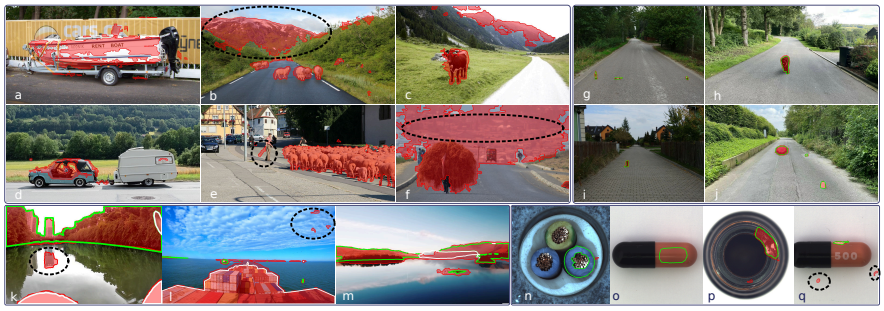


Fig. 4: Typical outputs with focus on "failure" cases. PixOOD anomalies are sometimes under-segmented (a) or over-segmented (b,c,m), but it often finds unexpected but reasonable anomalies: a stick (e), reflection in the water (k), birds (l), extra scratches (p), pill remains (q). It is also unable to detect logical anomalies like the switched cable in (n) or missing label in (o). Moreover, semantic/domain shifts are considered as anomaly: mountains (b,c), convertible roof with see-through (d) and city view (f) which are not present in the CityScapes. Legend: red - detected anomaly, green - GT when available, white - ignore region; ellipses mark relevant regions.

4.2 Road Anomaly Detection

We compare the proposed method with recent state-of-the-art methods on two standard datasets, Road Anomaly and FishyScapes LaF, and also on SMIYC benchmark designed for road anomaly segmentation task. Results on the standard datasets are presented and compared with most recent publications [16, 27, 34, 39] in Tab. 2. The proposed method outperforms other state-of-the-art methods (even several of those that utilise an auxiliary dataset to model the OOD data) often by large margin.

Evaluation results on the SMIYC benchmark are reported in Tab. 3. We report all three tracks, two for road anomaly detection (Obstacle Track and LaF NoKnown) and one for semantic segmentation anomaly detection (Anomaly Track). Compared to methods not utilising any auxiliary OOD data, our method is the best performing in Obstacle Track and second best in LaF NoKnown track.

To investigate the effect of a strong pre-trained representation (even though an extensive evaluation is out of the scope of this paper), we enhanced the DaCUP [39] method with the modern DINOv2 [30] ViT-L backbone. We denote the method as DaCUP++. In DaCUP++ we replace the DeepLabv3 segmentation part by the PixOOD classification MLP with the weights fixed and train the rest of DaCUP on CityScapes as in [39]. DaCUP++ improves most notably by decreasing the false positive rate in all experiments. The PixOOD remains competitive and outperforms the DaCUP++ on challenging scenarios of SMIYC.

Furthermore, since our method is generic (making no task specific design choices), it is of interest to try to incorporate DaCUP as a specialised module for a particular task. We added the DaCUP Reconstruction Module specialised for road anomaly detection as a second OOD detection head into PixOOD. The final anomaly score is a weighted average of PixOOD score (75%) and DaCUP

Table 3: Comparison with the state-of-the-art on the SMIYC [7] benchmark. For clarity, only top performing methods and main evaluation metrics are shown. The gray-out lines show the same comparison as in Tab. 2 (for details see Sec. 4.2).

Method	OOD Data	Anomaly Track			Obstacle Track			LaF NoKnown		
		AP ↑	FPR ↓	mean F1 ↑	AP ↑	FPR ↓	mean F1 ↑	AP ↑	FPR ↓	mean F1 ↑
SynBoost [11]	✓	56.44	61.86	9.99	71.34	3.15	37.57 ❶	81.71 ❷	4.64	48.72
ATTA [14]	✓	67.04	31.57	20.64	76.46	2.81	36.57	–	–	–
DenseHybrid [15]	✓	77.96	9.81	31.08	87.08	0.24	50.72 ❷	78.67 ❶	2.12	❶ 52.33
RPL+CoroCL [25]	✓	83.49	11.68	30.16	85.93	0.58	56.69	–	–	–
Maximized Entropy [8]	✓	85.47	15.00	28.72	85.07	0.75	48.51	77.90	9.70	❷ 49.92
Mask2Anomaly [34]	✓	88.72	14.63	47.16 ❷	93.22 ❷	0.20	❷ 68.15	–	–	–
EAM [16]	✓	❷ 93.75	❶ 4.09	❶ 60.86	92.87	0.52	❶ 75.58	–	–	–
RbA [27]	✓	❶ 94.46	❷ 4.60	❷ 51.87 ❶	95.12 ❶	0.08	57.44	–	–	–
ODIN [22]	✗	33.06	71.68	5.15	22.12	15.28	9.37	52.93	30.04	34.53
JSRNet [38]	✗	33.64	43.85	13.66	28.09	28.86	11.02	74.17	6.59	35.97
PEBAL [37]	✗	49.14	40.82	14.48	4.98	12.68	5.54	–	–	–
Image Resynthesis [24]	✗	52.28	25.93	12.51	37.71	4.70	8.38	57.08	8.82	19.17
Road Inpainting [23]	✗	–	–	–	54.14	47.12	36.01	82.93	35.75	❷ 52.25
NFlowJS [17]	✗	56.92	34.71	14.89	85.55 ❷	0.41	50.36 ❶	89.28 ❶	0.65	❶ 61.75
ObsNet [3]	✗	75.44	26.69	❷ 45.08	–	–	–	–	–	–
DaCUP [39]	✗	–	–	–	81.50	1.13	46.01	81.37	7.36	51.14
RbA [27]	✗	❷ 86.13	15.94	42.04 ❷	87.85	3.33	50.42	–	–	–
CSL [44]	✗	80.08 ❶	7.16	❶ 50.39	87.10	0.67	❶ 51.02	–	–	–
cDNP [13]	✗	❶ 88.90	❷ 11.42	28.12	–	–	–	–	–	–
PixOOD (**Ours**)	✗	68.88	54.33	19.82 ❶	88.90 ❶	0.30	❷ 50.82	❷ 85.07	❷ 4.46	44.41
DaCUP++ (CityScapes)	✗	–	–	–	86.10	0.90	44.61	79.47	3.40	37.60
Ours+DaCUP (recon.)	✗	–	–	–	84.96	0.93	39.44	87.57	1.29	48.97

module road anomaly score (25%). The resulting task-augmented PixOOD (denoted as "Ours+DaCUP (recon.)") significantly boosts the results of the PixOOD, outperforms DaCUP++ and shows that domain specific knowledge and generic OOD detection approach are complementary to a degree. Anomaly Track is the only experiment where PixOOD is "formally" under-performing; The typical observed failures are: (i) under-segmenting, (ii) detecting semantic shifts, such as mountains or forests which are nor annotated in Cityscapes dataset and (iii) detecting domain shift, *i.e.* same class as in Cityscapes but with very different appearance. The semantic/domain shifts may not be considered OOD in the Anomaly Track due to (vague) definition of anomaly and it requires an algorithm to generalize semantic concepts (like a car). Instead, our method detects anomalies w.r.t. the given ID data. This allows detecting these semantic/domain shifts, which is important in many tasks. For qualitative examples see Fig. 4.

4.3 Industrial Anomaly Detection

The industrial anomaly detection problem is most often addressed by training a model for each individual class (product). Only recently, new methods started to address the problem in a holistic manner by training a single model for all objects categories. PixOOD inherently falls into this category of a single unified model. The results for the standard MVTec AD [2] benchmark are shown in Tab. 4 and per category performance in the supplementary materials. PixOOD performs competitively to domain specialised method that use unified model.

Table 4: Comparison with the state-of-the-art on MVTec AD [2]. The methods are grouped by the use of a per-class models for each object category vs unified model. The bottom line shows results of combining PixOOD with specialised method DRAEM [43].

Method	per-object model	OOD Data	Image-level AUROC ↑	Pixel-level AUPRO ↑	Pixel-level AUROC ↑
PaDiM [10]	✓	✗	97.9	92.1	97.5
DRAEM [43]	✓	✓	98.0	92.8	97.3
DAF [6]	✓	✓	97.6	93.0	❷ 98.1
CFLOW-AD [19]	✓	✗	98.3	❶ 98.6	94.6
PatchCore (25%) [35]	✓	✗	❷ 99.1	93.4	❷ 98.1
PNI [1]	✓	✗	❶ 99.6	❷ 96.1	❶ 99.0
UniAD [42]	✗	✗	96.5	–	❷ 96.8
HVQ-Trans [26]	✗	✗	❶ 98.0	–	❶ 97.3
PixOOD (**Ours**)	✗	✗	❷ 97.0	91.3	94.6
Ours+DRAEM	✓	✓	98.6	95.3	98.0

Table 5: Comparison with the state-of-the-art on LaRS [45]. Results from official leaderboard (`https://lojzezust.github.io/lars-dataset/`) at the date of submission (considering latest model submissions from individual institutions; UniL - University of Ljubljana, UniC - University of Cagliary).

Model Name	**Q**	μ	Pr	Re	F1	mIoU
DeepLabv3 (UniL)	8 62.9	77.5	61.1	72.0	66.1	95.2
SegFormer (UniL)	7 67.8	78.6	63.8	77.5	70.0	96.8
Swin-T (UniL)	6 71.3	78.8	67.6	80.4	73.4	97.2
Mask2Former (HSU)	5 73.8	78.5	76.9	73.8	75.3	98.0
Mask2Former (DLMU)	3 75.7	78.4	79.7	75.1	77.3	97.8
Swin-L (HKUST)	❷ 77.8	79.6	78.5	82.0	80.2	97.1
Snarciv3 (UniC)	❶ 78.1	79.7	76.9	83.0	79.9	97.8
PixOOD (**Ours**)	4 73.9	74.6	70.7	81.6	75.8	97.5

Similarly to the road anomaly task, we can incorporate DRAEM [43] method domain specific knowledge to increase the performance for this specific task. The resulting task-augmented PixOOD (denoted as "Ours+DRAEM") improves the results (significantly in case of AUPRO metric).

4.4 Maritime Obstacle Detection

This experiment demonstrates the versatility of the proposed method in different settings and domains. The maritime obstacle detection problem is posed as semantic segmentation. The task is to segment the image into three classes – *Water, Sky and Obstacle*. During training, examples of all classes are available. To fit PixOOD to the setting, we model all three classes as in-distribution data and during the inference we use the classification network to produce class labelling. For each pixel and predicted class we then decide based on the OOD score if the pixel is ID (the class label remains as predicted) or OOD for which we change the class label to *Obstacle*. The results of our method are compared to stat-of-the-art methods (taking the latest version of the method submitted) from the official leaderboard and shown in Tab. 5. The proposed method performs favourably placing fourth place with the main issue being low precision due to over-segmentation (see Fig. 4 for qualitative examples).

5 Conclusions

In this paper we propose a novel pixel-level OOD detection method. The method is not designed for a specific task or benchmark, and it performs competitively on a range of pixel-level OOD problems. The method requires no OOD training samples, neither real nor synthetic. The method builds on a proposed data condensation algorithm which is theoretically linked to the optimisation of a complete data log likelihood in the EM algorithm. We applied the proposed method

to three very diverse pixel-level anomaly benchmarks and achieved state-of-the-art results on four out of seven considered datasets.

Acknowledgement This work was supported by Toyota Motor Europe and Czech Technical University in Prague institutional support Future Fund.

References

1. Bae, J., Lee, J.H., Kim, S.: PNI : Industrial Anomaly Detection using Position and Neighborhood Information. In: ICCV. pp. 6373–6383 (October 2023)
2. Bergmann, P., Fauser, M., Sattlegger, D., Steger, C.: MVTec AD – A Comprehensive Real-World Dataset for Unsupervised Anomaly Detection. In: CVPR (June 2019)
3. Besnier, V., Bursuc, A., Picard, D., Alexandre, B.: Triggering Failures: Out-Of-Distribution detection by learning from local adversarial attacks in Semantic Segmentation. In: ICCV (2021)
4. Blum, H., Sarlin, P.E., Nieto, J., Siegwart, R., Cadena, C.: The Fishyscapes Benchmark: Measuring Blind Spots in Semantic Segmentation. arXiv 1904.03215 (2019)
5. Bovcon, B., Muhovič, J., Vranac, D., Mozetič, D., Perš, J., Kristan, M.: MODS–A USV-Oriented Object Detection and Obstacle Segmentation Benchmark. ITS (2021). https://doi.org/10.1109/TITS.2021.3124192
6. Cai, Y., Liang, D., Luo, D., He, X., Yang, X., Bai, X.: A Discrepancy Aware Framework for Robust Anomaly Detection. IEEE Tran. Indust. Info. (2023). https://doi.org/10.1109/TII.2023.3318302
7. Chan, R., Lis, K., Uhlemeyer, S., Blum, H., Honari, S., Siegwart, R., Fua, P., Salzmann, M., Rottmann, M.: SegmentMeIfYouCan: A Benchmark for Anomaly Segmentation. In: NeurIPS Datasets and Bench. (2021)
8. Chan, R., Rottmann, M., Gottschalk, H.: Entropy Maximization and Meta Classification for Out-of-Distribution Detection in Semantic Segmentation. In: ICCV (October 2021)
9. Cho, M., Alizadeh-Vahid, K., Adya, S., Rastegari, M.: DKM: Differentiable k-Means Clustering Layer for Neural Network Compression. In: ICLR (2022), https://openreview.net/forum?id=J_F_qqCE3Z5
10. Defard, T., Setkov, A., Loesch, A., Audigier, R.: PaDiM: A Patch Distribution Modeling Framework for Anomaly Detection and Localization. In: ICPRW (2020)
11. Di Biase, G., Blum, H., Siegwart, R., Cadena, C.: Pixel-Wise Anomaly Detection in Complex Driving Scenes. In: CVPR (June 2021)
12. Dosovitskiy, A., Beyer, L., Kolesnikov, A., Weissenborn, D., Zhai, X., Unterthiner, T., Dehghani, M., Minderer, M., Heigold, G., Gelly, S., Uszkoreit, J., Houlsby, N.: An Image is Worth 16x16 Words: Transformers for Image Recognition at Scale. In: ICLR (2021), https://openreview.net/forum?id=YicbFdNTTy
13. Galesso, S., Argus, M., Brox, T.: Far Away in the Deep Space: Dense Nearest-Neighbor-Based Out-of-Distribution Detection. In: ICCVW (October 2023)
14. Gao, Z., Yan, S., He, X.: ATTA: Anomaly-aware Test-Time Adaptation for Out-of-Distribution Detection in Segmentation. In: NeurIPS (2023), https://openreview.net/forum?id=bGcdjXrU2w
15. Grcic, M., Bevandic, P., Segvic, S.: DenseHybrid: Hybrid Anomaly Detection for Dense Open-Set Recognition. In: ECCV (2022)
16. Grcić, M., Šarić, J., Šegvić, S.: On Advantages of Mask-Level Recognition for Outlier-Aware Segmentation. In: CVPRW (June 2023)

17. Grcić, M., Bevandić, P., Kalafatić, Z., Šegvić, S.: Dense Out-of-Distribution Detection by Robust Learning on Synthetic Negative Data. In: arXiv 2112.12833 (2023)
18. Gu, Z., Zhu, B., Zhu, G., Chen, Y., Tang, M., Wang, J.: AnomalyGPT: Detecting Industrial Anomalies using Large Vision-Language Models. arXiv preprint arXiv:2308.15366 (2023)
19. Gudovskiy, D., Ishizaka, S., Kozuka, K.: CFLOW-AD: Real-Time Unsupervised Anomaly Detection With Localization via Conditional Normalizing Flows. In: WACV. pp. 98–107 (January 2022)
20. Hendrycks, D., Gimpel, K.: Gaussian Error Linear Units (GELUs). arXiv 1606.08415 (2023)
21. Kingma, D.P., Ba, J.: Adam: A method for stochastic optimization. arXiv preprint arXiv:1412.6980 (2014)
22. Liang, S., Li, Y., Srikant, R.: Enhancing The Reliability of Out-of-distribution Image Detection in Neural Networks. In: ICLR (2018), https://openreview.net/forum?id=H1VGkIxRZ
23. Lis, K., Honari, S., Fua, P., Salzmann, M.: Detecting road obstacles by erasing them. In: arXiv 2012.13633 (2020)
24. Lis, K., Nakka, K., Fua, P., Salzmann, M.: Detecting the Unexpected via Image Resynthesis. In: ICCV (October 2019), https://infoscience.epfl.ch/record/269093?ln=en
25. Liu, Y., Ding, C., Tian, Y., Pang, G., Belagiannis, V., Reid, I., Carneiro, G.: Residual Pattern Learning for Pixel-Wise Out-of-Distribution Detection in Semantic Segmentation. In: ICCV (October 2023)
26. Lu, R., Wu, Y., Tian, L., Wang, D., Chen, B., Liu, X., Hu, R.: Hierarchical Vector Quantized Transformer for Multi-class Unsupervised Anomaly Detection. In: NeurIPS (2023), https://openreview.net/forum?id=clJTNssgn6
27. Nayal, N., Yavuz, M., Henriques, J.F., Güney, F.: RbA: Segmenting Unknown Regions Rejected by All. In: ICCV (2023)
28. Neyman, J., Pearson, E.S.: On the use and interpretation of certain test criteria for purposes of statistical inference. Biometrika (1928)
29. Neyman, J., Pearson, E.S.: Ix. on the problem of the most efficient tests of statistical hypotheses. Philosophical Transactions of the Royal Society of London. Series A, Containing Papers of a Mathematical or Physical Character (1933)
30. Oquab, M., Darcet, T., Moutakanni, T., Vo, H.V., Szafraniec, M., Khalidov, V., Fernandez, P., Haziza, D., Massa, F., El-Nouby, A., Howes, R., Huang, P.Y., Xu, H., Sharma, V., Li, S.W., Galuba, W., Rabbat, M., Assran, M., Ballas, N., Synnaeve, G., Misra, I., Jegou, H., Mairal, J., Labatut, P., Joulin, A., Bojanowski, P.: Dinov2: Learning robust visual features without supervision (2023)
31. Pinggera, P., Ramos, S., Gehrig, S., Franke, U., Rother, C., Mester, R.: Lost and found: detecting small road hazards for self-driving vehicles. In: IROS (2016)
32. R. H. Byrd, P.L., Nocedal, J.: A Limited Memory Algorithm for Bound Constrained Optimization. SIAM Jour. on Scien. and Stat. Comp. (1995)
33. Radford, A., Kim, J.W., Hallacy, C., Ramesh, A., Goh, G., Agarwal, S., Sastry, G., Askell, A., Mishkin, P., Clark, J., et al.: Learning transferable visual models from natural language supervision. In: ICML. pp. 8748–8763 (2021)
34. Rai, S.N., Cermelli, F., Fontanel, D., Masone, C., Caputo, B.: Unmasking Anomalies in Road-Scene Segmentation. In: ICCV (October 2023)
35. Roth, K., Pemula, L., Zepeda, J., Schölkopf, B., Brox, T., Gehler, P.: Towards Total Recall in Industrial Anomaly Detection. In: CVPR. pp. 14318–14328 (2022)
36. Schlesinger, M.I., Hlavac, V.: Ten Lectures on Statistical and Structural Pattern Recognition. Computational Imaging and Vision (2002)

37. Tian, Y., Liu, Y., Pang, G., Liu, F., Chen, Y., Carneiro, G.: Pixel-wise Energy-biased Abstention Learning for Anomaly Segmentation on Complex Urban Driving Scenes. In: ECCV (2021)
38. Vojir, T., Šipka, T., Aljundi, R., Chumerin, N., Reino, D.O., Matas, J.: Road Anomaly Detection by Partial Image Reconstruction With Segmentation Coupling. In: ICCV (2021)
39. Vojíř, T., Matas, J.: Image-Consistent Detection of Road Anomalies As Unpredictable Patches. In: WACV (2023)
40. Vojíř, T., Šochman, J., Aljundi, R., Matas, J.: Calibrated Out-of-Distribution Detection with a Generic Representation. In: ICCVW (October 2023)
41. Wang, H., Li, Y., Yao, H., Li, X.: CLIPN for Zero-Shot OOD Detection: Teaching CLIP to Say No. In: ICCV (October 2023)
42. You, Z., Cui, L., Shen, Y., Yang, K., Lu, X., Zheng, Y., Le, X.: A Unified Model for Multi-class Anomaly Detection. In: NeurIPS (2022)
43. Zavrtanik, V., Kristan, M., Skocaj, D.: DRAEM - A Discriminatively Trained Reconstruction Embedding for Surface Anomaly Detection. In: ICCV (2021)
44. Zhang, H., Li, F., Qi, L., Yang, M.H., Ahuja, N.: CSL: Class-Agnostic Structure-Constrained Learning for Segmentation Including the Unseen. Proc. of the AAAI Conf. on Artif. Intell. **38**(7) (2024). https://doi.org/10.1609/aaai.v38i7.28535
45. Žust, L., Perš, J., Kristan, M.: LaRS: A Diverse Panoptic Maritime Obstacle Detection Dataset and Benchmark. In: ICCV (2023)

A Social, Ethics and Privacy Impact and Considerations

We thank anonymous **Reviewer #1** for bringing these concerns to our attention:

> *The authors state that there is no potential negative societal impact in their research. However, thinking about a real-world deployment of the model proposed for, e.g., anomaly detection in video surveillance scenarios, I think it would be nice to briefly discuss ethical, privacy, transparency and fairness concerns in this paper.*

In response, we considered and discussed the issue broadly. No immediate privacy or ethical issues with the current pixel-level method were identified. On the contrary, we argue that enhancing deployed models with the ability to output the "I do not know" label is beneficial for AI systems in general. Representing decision uncertainty partially mitigates the lack of diversity in datasets, potential biases, and it avoids non-confident or wrong over-confident decisions in downstream tasks by identifying these cases as out-of-distribution (OOD).

We, however, agree that in a future research there may arise privacy and ethical concerns regarding applications in domains such as face re-identification and recognition, surveillance, or behavior and action analysis. It is possible that a method, similar to the proposed PixOOD, could potentially be exploited for nefarious applications. For example, penalizing "not approved" (thus not in the training data and identified as OOD) types of behavior or actions performed under surveillance. The proposed method is currently not directly applicable in such settings and the adaptation, in our expert opinion, is non-trivial.

We keep these risks in mind, noting that every tool can be used in both socially beneficial or harmful ways.

B Additional Quantitative Results

Additional results on the SMIYC benchmark for all tracks and all metrics are reported in Tab. 7 and per-class results of the proposed PixOOD method on the MVTec AD benchmark are reported in Tab. 6.

Table 6: Per-object results of the proposed PixOOD method on the MVTec AD [2] benchmark.

	Class	Image-level	Pixel-level	
		AUROC ↑	AUPRO ↑	AUROC ↑
Objects	bottle	100.00	96.65	98.84
	cable	93.39	90.05	95.51
	capsule	94.815	95.83	97.36
	hazelnut	99.89	98.16	99.40
	metal nut	100.00	92.62	96.64
	pill	96.37	95.15	87.90
	screw	83.05	87.20	95.99
	toothbrush	92.5	66.94	73.83
	transistor	97.33	75.61	89.75
	zipper	98.77	87.46	94.96
Textures	carper	99.40	96.80	99.01
	grid	100.00	98.27	99.61
	leather	100.00	99.13	99.40
	tile	100.00	93.87	97.21
	wood	99.47	95.23	93.16

C Additional Qualitative Results

We present additional qualitative results for road anomaly detection in Fig. 5, industrial anomaly detection in Fig. 6 and maritime obstacle detection in Fig. 7.

Table 7: Comparison with the state-of-the-art on SMIYC [7] benchmark.

Method	OOD Data	Anomaly Track					Obstacle Track					LostAndFound NoKnown				
		AP ↑	FPR ↓	sIoU gt ↑	PPV ↑	mean F1 ↑	AP ↑	FPR ↓	sIoU gt ↑	PPV ↑	mean F1 ↑	AP ↑	FPR ↓	sIoU gt ↑	PPV ↑	mean F1 ↑
SynBoost [11]	✓	56.44	61.86	34.68	17.81	9.99	71.34	3.15	44.28	41.75	37.57	81.71	4.64	36.83	72.32	48.72
ATTA [14]	✓	67.04	31.57	44.58	29.55	20.64	76.46	2.81	43.93	37.66	36.57	–	–	–	–	–
DenseHybrid [15]	✓	77.96	9.81	54.17	24.13	31.08	87.08	0.24	45.74	50.10	50.72	78.67	2.12	46.90	52.14	52.33
RPL+CoroCL [25]	✓	83.49	11.68	49.77	29.96	30.16	85.93	0.58	52.62	56.65	56.69	–	–	–	–	–
Maximized Entropy [8]	✓	85.47	15.00	49.21	39.51	28.72	85.07	0.75	47.87	62.64	48.51	77.90	9.70	45.90	63.06	49.92
Mask2Anomaly [34]	✓	88.72	14.63	55.28	51.68	47.16	93.22	0.20	55.72	75.42	68.15	–	–	–	–	–
EAM [16]	✓	93.75	4.09	67.09	53.77	60.86	92.87	0.52	65.86	76.50	75.58	–	–	–	–	–
RbA [27]	✓	94.46	4.60	64.93	47.51	51.87	95.12	0.08	54.34	59.08	57.44	–	–	–	–	–
ODIN [22]	✗	33.06	71.68	19.53	17.88	5.15	22.12	15.28	21.62	18.50	9.37	52.93	30.04	39.79	49.33	34.53
JSRNet [38]	✗	33.64	43.85	20.20	29.27	13.66	28.09	28.86	18.55	24.46	11.02	74.17	6.59	34.28	45.89	35.97
PEBAL [37]	✗	49.14	40.82	38.88	27.20	14.48	4.98	12.68	29.91	7.55	5.54	–	–	–	–	–
Image Resynthesis [24]	✗	52.28	25.93	39.68	10.95	12.51	37.71	4.70	16.61	20.48	8.38	57.08	8.82	27.16	30.69	19.17
Road Inpainting [23]	✗	–	–	–	–	–	54.14	47.12	57.64	39.50	36.01	82.93	35.75	49.21	60.67	52.25
NFlowJS [17]	✗	56.92	34.71	36.94	18.01	14.89	85.55	0.41	45.53	49.53	50.36	89.28	0.65	54.63	59.74	61.75
ObsNet [3]	✗	75.44	26.69	44.22	52.56	45.08	–	–	–	–	–	–	–	–	–	–
DaCUP [39]	✗	–	–	–	–	–	81.50	1.13	37.68	60.13	46.01	81.37	7.36	38.34	67.29	51.14
RbA [27]	✗	86.13	15.94	56.26	41.35	42.04	87.85	3.33	47.44	56.16	50.42	–	–	–	–	–
CSL [44]	✗	80.08	7.16	46.46	50.02	50.39	87.10	0.67	44.70	53.13	51.02	–	–	–	–	–
cDNP [13]	✗	88.90	11.42	50.44	29.04	28.12	–	–	–	–	–	–	–	–	–	–
PixOOD (**Ours**)	✗	68.88	54.33	44.15	24.32	19.82	88.90	0.30	42.68	57.49	50.82	85.07	4.46	30.18	78.47	44.41



Fig. 5: Road anomaly detection examples.

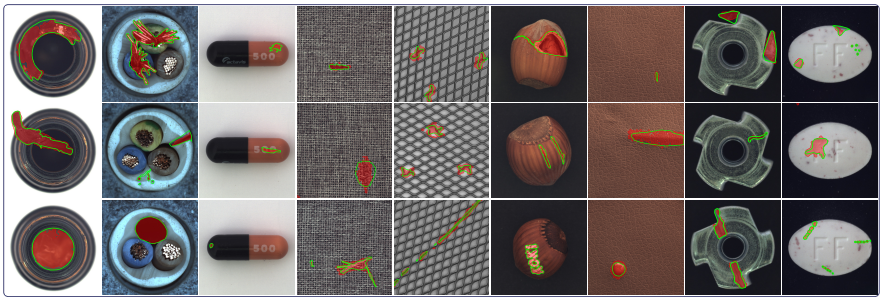


Fig. 6: Industrial MVTec AD detection examples.

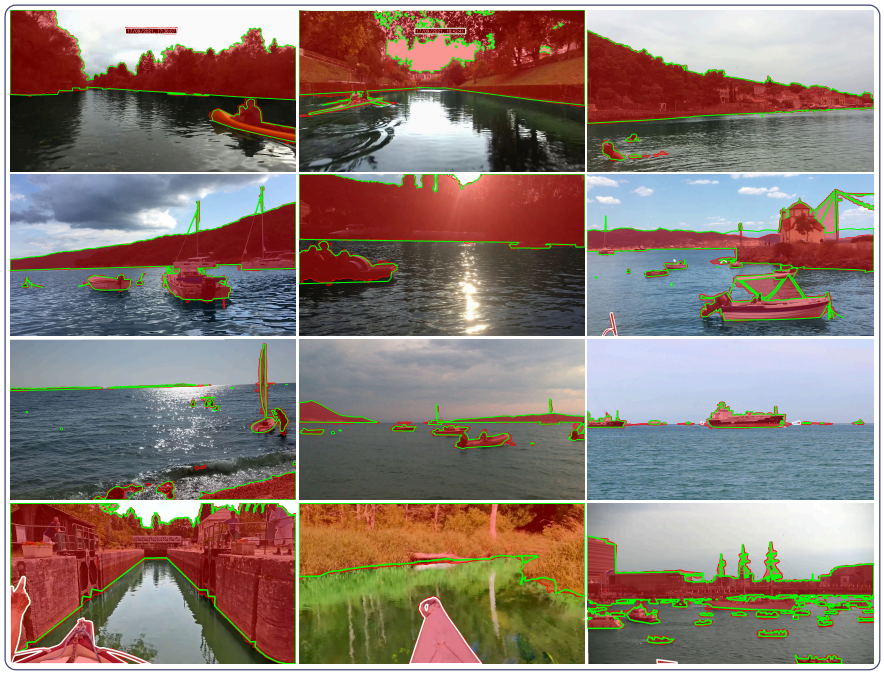


Fig. 7: Maritime Obstacle (LaRS) anomaly detection examples.